Studies Toward Optimizing Selection Criteria for Top Quark Pair Production in Association with a Vector Boson at ATLAS

Eric Scotti

Spring 2015

Honors Thesis
Department of Physics
Duke University

Approved By:

Advisor: Mark Kruse, Ph.D

Reader: Ashutosh Kotwal, Ph.D

Reader: Chris Walter, Ph.D

Abstract

The Large Hadron Collider (LHC) in Switzerland is scheduled to turn on again in the middle of 2015 at unprecedented proton-proton collision energies of 13 TeV, to begin the so-called "Run 2" which will last several years. One of the main goals will be to measure the Higgs coupling to top quarks by searching for top quark pair production ($t\bar{t}$) in association with a Higgs boson ($pp \to t\bar{t}H$). An important milestone toward this measurement will be to measure top quark pair production in association with a vector boson ($pp \to t\bar{t}W$ and $pp \to t\bar{t}Z$). These processes have recently been observed at the LHC. Here we discuss these processes in terms of the many different final states available and how one might optimize the selection for them using the ATLAS detector at the LHC. We find that requiring at least one b-jet in the event removes much of the background processes, and that the trilepton final state is optimal for selecting either of $t\bar{t}W$ and $t\bar{t}Z$, and the same sign dilepton state is best for finding $t\bar{t}V$ where V is either of W or Z.

Contents

List of Figures

List of Tables

1 The Standard Model of Particle Physics

The current overarching theory of particle physics is known as the Standard Model of Particle Physics, which describes the basic building blocks of matter and the dominant forces at small distances. In this theory all matter is composed of elementary particles called leptons and quarks which interact through the exchange of mediators called vector bosons. There are six leptons, along with their respective antiparticles, which can be broken into three generations which have similar properties. In each family the charge of the more massive particle is -1, while it's associated neutrino is chargeless and much less massive. The families differ from each other by mass, though the masses of the neutrinos are not currently known, with each higher generation being more massive than the previous. The first family is the electron and electron neutrino, followed by the muon and muon neutrino, and finally the tau and tau neutrino. The electron is also the only stable charged particle across the generations. Each of these particles also has an associated antiparticle which has an identical mass but flipped signs for charge and lepton number. These generations are also summarized in the Table 1.

Flavor	Generation	Mass (MeV/c^2)	Electric Charge (e)
Electron (e^-)	1	0.511	-1
Electron Neutrino (ν_e)	1	$< 7 \times 10^{-6}$	0
Muon (μ^-)	2	106	-1
Muon Neutrino (ν_μ)	2	< 0.3	0
Tau (τ^-)	3	1777	-1
Tau Neutrino (ν_τ)	3	< 30	0

Table 1: The Three Generations of Leptons

Under the standard model, the leptons only interact via the electromagnetic and weak forces. In these interactions the standard model imposes a conservation of lepton number, such that the total number of leptons minus the number of antileptons is preserved between interactions. In most cases the different family lepton numbers will also be conserved in interactions, however due to neutrinos having a nonzero mass, they can undergo oscillations between types. For our purposes however this effect will be negligible and we can assume a conservation of each type of lepton number as well.

The six types of quarks are similarly divided into three generations of increasing mass. In each generation their is an "up-like" quark with a charge of 2/3 and a

"down-like" quark with a charge of $-1/3$. The three families are the up and down quarks, the strange and charm quarks, and the top and bottom quarks. Each quark also has an additional quantity associated with its flavor; strangeness for the strange quark, charm for the charm quark, and likewise for the others. As with the leptons, each quark has an associated antiquark with the same mass but an opposite sign for all other values. These generations are summarized in Table 2.

Flavor	Generation	Mass (MeV/c^2)	Electric Charge (e)
Up (u)	1	$2.3^{+0.1}_{-0.5}$	2/3
Down (d)	1	$4.8^{+0.5}_{-0.3}$	-1/3
Charm (c)	2	1275 ± 25	2/3
Strange (s)	2	95 ± 5	-1/3
Top (t)	3	173210 ± 510	2/3
Bottom (b)	3	4180 ± 30	-1/3

Table 2: The Three Generations of Quarks

Each quark has one of three colors (red,green,blue), essentially three types of "charge" that is acted upon by the strong force. Quarks, unlike other particles, have never been observed by themselves but always bond together by the strong force into either baryons or mesons. Baryons are collections of three quarks, one of each color, while mesons are a bound-state between a quark and anti-quark of a corresponding color and anti-color. Similarly to the leptons, there are also flavor conservation laws for the quarks, however unlike the leptons these laws only hold for strong, and electromagnetic interactions. Weak interactions break these conservations laws, and it was this property that originally motivated its discovery. One quark of particular interest for this study is the top quark. It has a mass over 40 times larger than the next massive quark, the bottom quark, with which it shares its generation. Due to this greatly increased mass the top quark also decays faster than it can hadronize, and as such there are no baryons or mesons made with top quarks. [1]

The third type of particle, the mediators, are the particles responsible for each of the three major forces included in the Standard Model. Gravity is excluded from the standard model, and is well described by the theory of general relativity. These two theories have yet to be reconciled with each other, however due to the small masses in particle physics the effects of gravity are negligible. The forces described by the standard model are manifested as the exchange of mediator particles between two interacting particles. These mediators are: the photon for the electromagnetic force, the W and Z bosons for the weak force, and the gluon for the strong force.

The final particle in the Standard Model is the Higgs boson. It is the manifestation of the Higgs field, which is theorized to give rise to the mass of all the elementary particles. Particles that interact more strongly with the field have higher masses and those with weaker interactions have lower masses.

2 The Large Hadron Collider and CERN

The Large Hadron Collider (LHC) at CERN is currently the largest proton-proton collider in the world. The LHC accelerates bunches of $\sim 10^{10}$ protons, with a bunch spacing of 50 ns, in both directions along its 4.3 kilometer radius circular track. These bunches are then collided together in the detectors located along the LHC ring. During it's first run the LHC reached a center of mass energy of 7 TeV and later 8 TeV. It is currently preparing for Run 2, to begin Spring 2015, where it will reach a center of mass energy of 14 TeV. This paper looks at data modeling the 8 TeV events produced at the LHC and recorded by the ATLAS detector in 2012. During this period the peak instantaneous luminosity was $7.7 \times 10^{33} cm^2 s^{-1}$ with a total of $21.7 fb^{-1}$ of data collected by the ATLAS detector.

3 The ATLAS Detector

ATLAS is a multipurpose particle physics detector that has cylindrical and backward-forward symmetries (see Figure 1). It consists of three main subsystems: an inner detector surrounded by a superconducting solenoid, electromagnetic and hadronic calorimeters, and a muon spectrometer. The inner detector is immersed in a 2 T magnetic field in the axial direction and provides tracking information for charged particles using silicon pixel and microstrip detectors in the pseudorapidity range $|\eta| < 2.5$, and a transition radiation tracker (TRT) that tracks out to $|\eta| < 2.0$. The electromagnetic calorimeter uses lead absorbers with liquid argon (LAr) as the active material and covers the region $|\eta| < 3.2$, in two pieces; a barrel region for $|\eta| < 1.475$ and an end-cap region for $1.375 < |\eta| < 3.2$. The hadronic calorimeter uses two different types of detectors; a steel/scintillator-tile detector sitting directly outside of the electromagnetic calorimeter covering the barrel region of $|\eta| < 1.7$, and an end-cap region covering $1.5 < |\eta| < 4.2$ using LAr as the active material and copper absorbers. The muon spectrometer measures the deflection of muons in the magnetic field produced by the large superconducting toroidal magnets in the region $|\eta| < 2.7$. [2] [4]

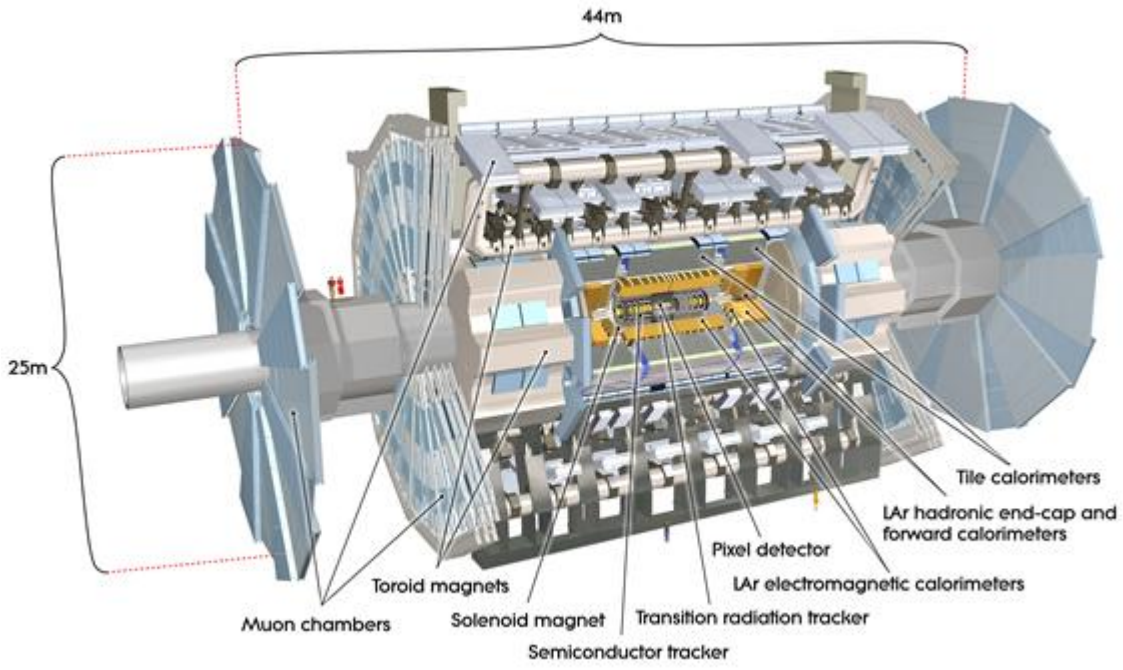

Figure 1: Schematic Diagram of the ATLAS Detector

3.1 Coordinate Basis and Variable Definitions

The ATLAS detector uses a right handed coordinate system. The origin is at the center of the detector at the nominal interaction point, with the z axis pointing along the direction of the beam pipe. The x and y directions point towards the center of the LHC ring and upwards respectively. The typical cylindrical coordinates (r, ϕ) are used in the transverse plane of the detector. The pseudorapidity η is used instead of the polar angle θ, and is defined as η = -ln(tan(θ/2)).

This study looks at a number of kinematic variables used to characterize an event. These variables are:

Transverse Momentum (p_T): The momentum of a particle or jet in the transverse plane of the detector. The reason for using the projection of the momentum into the transverse plane is that the initial value of the transverse momentum of the system is known to be zero due to the colliding protons moving in the longitudinal direction. The total momentum and longitudinal momentum are not used because the initial value for the system cannot be determined. Each proton is made up of a collection of particles each with a fraction of the total energy and momentum of the proton,

and when two protons collide, it is actually two of these parts colliding, and so the true momentum and energy in the collisions is unknown.

Missing Transverse Energy (MET): The total momentum after a collision is known to be zero from conservation of momentum/energy, however it is possible for particles to escape the detector without being recorded. The typical candidates for escaping are the neutrinos, as they rarely interact with matter. The MET is a measure of the energy that is missing due to these escaped particles, which cause the total momentum after the collision to not be equal to zero. Muons also escape the detector, carrying away energy, however their momentum can be determined using tracking information, and this escaped energy can be corrected for accordingly.

Number of Jets (N_{jets}): When a particle decays into quarks, they will hadronize, creating a stream of hadrons called a jet. This variable records the number of such occurrences in a given event.

Number of b tagged Jets (N_{bjets}): Same as N_{jets} however this time it is required that the jet is formed from a b quark, determined by a given "b-tagging" algorithm.

Distance Between Objects(ΔR): A measure of the distance between two objects in the $\eta - \phi$ coordinate system of the detector given by $\sqrt{\Delta\eta^2 + \Delta\phi^2}$.

4 Motivation

The top quark, first discovered in 1995 by the D0 and CDF collaborations [2] is the heaviest of the elementary particles. The top quark is unique in that its large mass causes it to decay faster ($\sim 10^{-25}s$) than it can hadronize ($\sim 10^{-24}s$) and unlike other quarks will not produce jets. The top quark also has non-zero couplings to bosons (γ, W, Z, g, H), which are inferred from various analyses of top production (though $t\bar{t}H$ has yet to be observed). The very large mass of the top quark indicates a strong coupling to the Hiss boson, possibly indicating a connection to electroweak symmetry breaking, as yet unknown, that could be an avenue to new physics. [2], [3] This paper looks at the top pair production in association with the W and Z bosons, ($t\bar{t}W$,$t\bar{t}Z$). These processes can be used to test the consistency of the standard model, but also in searches for new physics, as different theories can produce different coupling strengths with the top quark. An understanding of these two processes is also important for further testing of the Higgs coupling with the top quark, as they form a significant background to the $t\bar{t}H$ process

5 Methods

The analysis performed in this study is broken roughly into two parts. First the theoretical cross sections and branching ratios for the two processes and major background processes are used to determine the best final states to consider, when trying to separate these processes from the background. The second part uses Monte Carlo generated samples, to look at the kinematic quantities described in Section 3.1, and find combinations of these quantities that can be used to separate our signal processes from the background using a neural network.

5.1 Theoretical Final States

In order to determine the theoretically best final states to consider when looking for $t\bar{t}+W$ or Z processes we first used the branching ratios of each type of starting and intermediate particles, shown in Table 3. [5] These branching ratios were used to

Decay	BR(%)
t	
$\rightarrow Wb$	≈ 100
W	
$\rightarrow e\nu$	10.71
$\rightarrow \mu\nu$	10.63
$\rightarrow \tau\nu$	11.38
$\rightarrow hadrons$	67.41
Z	
$\rightarrow e^+e^-$	3.363
$\rightarrow \mu^+\mu^-$	3.366
$\rightarrow \tau^+\tau^-$	3.370
$\rightarrow \nu\nu$	20.00
$\rightarrow b\bar{b}$	15.12
$\rightarrow hadrons$	39.23
τ	
$\rightarrow e\nu_e\nu_\tau$	17.83
$\rightarrow \mu\nu_\mu\nu_\tau$	17.41
$\rightarrow nonleptonic$	64.76

Table 3: Branching ratios for individual particle decays

determine all of the possible final states and their probability for each of the processes looked at. These final states are also broken down into distinct groups:

Opposite sign dilepton (OSD): containing two oppositely charged muons or electrons, and is also further broken down into the three categories of $ee, e\mu, \mu\mu$.

Same sign dilepton (SSD): containing two muons or electrons of the same charge, and is also further broken down into three categories of $ee, e\mu, \mu\mu$.

Opposite sign trilepton (OST): containing three muons or electrons one of which has an opposite charge to the other two, and is also further broken down into $eee, ee\mu, e\mu\mu, \mu\mu\mu$.

Same sign trilepton (SST): containing three muons or electrons all of which have the same charge, and is also further broken down into $eee, ee\mu, e\mu\mu, \mu\mu\mu$.

The number of b jets (N_{bjets}) in each final state is also considered by looking at the number of b or $\bar{b}$ quarks that are in the final state. The effect on the ratios of final states between processes is considered for $N_{bjets} \geq 0$, $N_{bjets} = 0$, $N_{bjets} = 1$, $N_{bjets} = 2$, and $N_{bjets} > 2$.

The breakdown of the final states is considered under three sets of conditions: theory, after cuts on η, and after an addition cut on p_T. The first is simply the theoretical values that should be observed if all events produced were detected. However the ATLAS detector can only observe events within a certain η range for a given type of particle, typically only within $|\eta| < 2.5$. Truth level Monte Carlo data is used in order to estimate the probability of a given type of particle falling within the η range for which the ATLAS detector will be able to observe it. This is done by taking the ratio of the number of particles of a given type that fall within the proper η to the total number of particles of that type. In addition to this η cut the final states are also considered for different cuts on p_T. Similarly to the η cuts, Monte Carlo truth data is used to estimate the probability of a particle having a large enough p_T to pass the cut. All of the probabilities for the p_T cut are considered only for particles that have already passed the cuts η.

After the breakdown of the final states for each process is found, the theoretical cross sections for each process (see Table 4) are used to compare them against each other. The cross section is a measure of the probability of a given process being produced from the initial proton-proton collision. These cross sections are used as weights when comparing the percentages of each type of final state contributed by each process, so that the expected number of events classified as each process can be taken into account in the comparison.

For this study the best final states to consider will be those with the largest proportion of events coming from our signal processes of $t\bar{t}W$ and $t\bar{t}Z$.

Process	$\sqrt{s}$	$\sigma(pb)$	Source
Signal			
$t\bar{t}W$	8 TeV	$0.232 \pm .051$	ATLAS-CONF-2014-038
$t\bar{t}Z$	8 TeV	$0.206 \pm .045$	ATLAS-CONF-2014-038
Background			
$t\bar{t}$	8 TeV	$252.9^{+13.3}_{-14.5}$	arXiv:1406.5375[hep-ex]
WZ	8 TeV	20.3 ± 0.8	ATLAS-CONF-2013-021
ZZ	8 TeV	$7.2^{+0.3}_{-0.2}$	ATLAS-CONF-2013-020

Table 4: Cross sections for signal and background processes.

5.2 Distinguishing $t\bar{t}W$ and $t\bar{t}Z$ from Background

Once we have determined the best type of final state to consider for finding $t\bar{t}W$ and $t\bar{t}Z$ processes, we started to look at kinematic quantities and cuts that could be used to further distinguish the signal events from the background events. The kinematic quantities of interest are described in Section 3.1. These kinematic quantities are estimated using truth level information from Monte Carlo generated samples for $t\bar{t}W$, $t\bar{t}Z$, $t\bar{t}$, and WZ. These samples were generated using madgraph with pythia for $t\bar{t}W$ and $t\bar{t}Z$, Powheg with pythia for $t\bar{t}$. The goal is to look at varying combinations of these variables in an attempt to find a phase space that separates our signal events from the background, so that both regions can be simultaneously measured, or to determine possible cuts on the variables that can isolate the signal events and remove most of the background processes.

To better estimate the distributions of the kinematic quantities that would be observed in the ATLAS detector, addition selection criteria were imposed on the particles. In order to be selected, a particle must have had a parent particle that was in the process of interest, and must pass a cut p_T and a cut on η corresponding to the observable range of the detector. These cuts for each particle type are as follows:

Electron: an electron is required to have $p_T > 25GeV$ and $|\eta| < 2.47$ but not between $1.37 < |\eta| < 1.52$. This second excluded region is a requirement of the ATLAS detector as the this $/eta$ range is not instrumented in the calorimeter.

Muon: a muon is required to have $p_T > 25GeV$ and $|\eta| < 2.5$.

Jets: jets are required to have $p_T > 25GeV$ and $|\eta| < 4$.

b-jets: b-jets are required to have $p_T > 25GeV$ and $|\eta| < 2.5$.

neutrinos: neutrinos do not have any additional cuts as they are unable to be detected by the ATLAS detector and are the primary contribution to MET.

6 Results

Here the results of the study are presented. First the results for the best theoretical final state will be presented, followed by the results of the kinematic study.

6.1 Theoretical Final States

An example of the results for the branching ratios of our two signal processes are given in Table 5 and Table 6. The first thing to note is that in both $t\bar{t}W$ and

	Decay	Relative BR	Relative BR (η)	relative BR (p_T and η)
$t\bar{t}W$	efficiencies	1.0000	0.8228	0.5114
$t\bar{t}W \rightarrow$	ll	0.8985	0.9107	0.9337
	$l^{\pm}l^{\mp}$ (OS)	0.5989	0.6123	0.6243
	$e^{\pm}e^{\mp}$	0.1513	0.1457	0.1489
	$e^{\pm}\mu^{\mp}$	0.2995	0.3060	0.3120
	$\mu^{\pm}\mu^{\mp}$	0.1482	0.1607	0.1634
	$l^{\pm}l^{\pm}$ (SS)	0.2995	0.2984	0.3094
	$e^{\pm}e^{\pm}$	0.0756	0.0709	0.0736
	$e^{\pm}\mu^{\pm}$	0.1498	0.1491	0.1546
	$\mu^{\pm}\mu^{\pm}$	0.0741	0.0784	0.0812
$t\bar{t}W \rightarrow$	lll	0.1015	0.0893	0.0663
	$OSlll$	0.1015	0.0893	0.0663
	$OSeee$	0.0129	0.0103	0.0077
	$OSee\mu$	0.0383	0.0326	0.0243
	$OSe\mu\mu$	0.0379	0.0343	0.0254
	$OS\mu\mu\mu$	0.0125	0.0120	0.0089
	$SSlll$	0.0000	0.0000	0.0000
	$SSeee$	0.0000	0.0000	0.0000
	$SSee\mu$	0.0000	0.0000	0.0000
	$SSe\mu\mu$	0.0000	0.0000	0.0000
	$SSe\mu\mu$	0.0000	0.0000	0.0000

Table 5: Branching ratios for $t\bar{t}W$ with 25 GeV cut on p_T

$t\bar{t}Z$ there are not any same sign trilepton states. This is also true of our background processes and thus for the rest of this paper the same sign trilepton region will be ignored and the opposite sign trilepton region will be referred to as the trilepton

	Decay	Relative BR	Relative BR (η)	relative BR (p_T and η)
$t\bar{t}Z$	efficiencies	1.0000	0.8716	0.6113
$t\bar{t}Z \rightarrow$	ll	0.7709	0.7914	0.8296
	$l^{\pm}l^{\mp}$ (OS)	0.7471	0.7483	0.7545
	$e^{\pm}e^{\mp}$	0.2647	0.2513	0.2613
	$e^{\pm}\mu^{\mp}$	0.2200	0.2200	0.2077
	$\mu^{\pm}\mu^{\mp}$	0.2623	0.2769	0.2855
	$l^{\pm}l^{\pm}$ (SS)	0.0238	0.0431	0.0750
	$e^{\pm}e^{\pm}$	0.0061	0.0116	0.0188
	$e^{\pm}\mu^{\pm}$	0.0119	0.0216	0.0375
	$\mu^{\pm}\mu^{\pm}$	0.0058	0.0099	0.0187
$t\bar{t}Z \rightarrow$	lll	0.2291	0.2086	0.1704
	$OSlll$	0.2291	0.2086	0.1704
	$OSeee$	0.0550	0.0454	0.0368
	$OSee\mu$	0.0597	0.0536	0.0446
	$OSe\mu\mu$	0.0601	0.0567	0.0468
	$OS\mu\mu\mu$	0.0543	0.0529	0.0422
	$SSlll$	0.0000	0.0000	0.0000
	$SSeee$	0.0000	0.0000	0.0000
	$SSee\mu$	0.0000	0.0000	0.0000
	$SSe\mu\mu$	0.0000	0.0000	0.0000
	$SSe\mu\mu$	0.0000	0.0000	0.0000

Table 6: Branching ratios for $t\bar{t}Z$ with 25 GeV cut on p_T

region. In practice the same sign trilepton events can occur due to the charges of leptons being misidentified by the detector, however these effects are not considered in this study. Second is that the trilepton final state is more common in $t\bar{t}Z$ at approximately 22% of all events, than in $t\bar{t}W$ where only about 10% of events have a trilepton final state. However both of these processes have predominately opposite sign dilepton final states, with only about 30% of events being in the same sign dilepton region for $t\bar{t}W$ and less than 5% for $t\bar{t}Z$. Finally the differences in lepton types is largely negligible as the rates for leptons of the same type are roughly equivalent, with the mixed types being approximately twice as common for dilepton events and three times as common for trilepton events as would be expected from combinatorial arguments.

The first calculated column of Tables 5 and 6 give the purely theoretical pro-

portions one would expect from the particle Branching Ratios given in Table 3 if every event could be recorded in the detector. The next two columns seek to estimate the proportions given the constraints of the detector, and a common cut on p_T. The ATLAS detector is unable to record events with a large forward direction along the beam, approximately $|\eta| > 2.5$. The η efficiencies were estimated using truth level data from Monte Carlo simulations, and finding the proportion of leptons that fall within the detectable η range of the particle (see Section 5.2. The proportions falling within the detector ranges were found to be roughly equivalent for electrons and muons, but varied slightly between the initial particles (t, W, Z). For a first approximation of the η cut, it was assumed that the probability of a lepton being outside of the η range depended only on the initial particle and not the intermediate decays. It was found that approximately 82% of events for $t\bar{t}W$ and 87% of events for $t\bar{t}Z$ fell within the η range of the detector. The proportion of leptons passed for a given cut on p_T was similarly estimated from Monte Carlo truth data for each of the initial particles after the previous η cuts were applied. The probability of a lepton being excluded was again found to be approximately the same for electrons and muons and varying slightly for each of the initial particles. Again for a first order estimate it was assumed that the probability of being cut was independent of the number of intermediary decays from the initial particle. It was found that for our primary cut of 25 GeV on p_T, which we will be using for our selection criteria, that only approximately 51% and 61% of leptons will be detected and selected for $t\bar{t}W$ and $t\bar{t}Z$ respectively. As one might expect, the proportion of dilepton events increases as more constraints are placed on the theoretical values as some of the trilepton events will become dilepton events when one of their leptons is excluded.

Table 7 shows the comparisons between the signal and background processes before any cuts are made for $N_{bjets} \geq 0$. As previously seen in Table 4 the cross sections for our signal regions are much smaller than those of the background, and as such they are often overshadowed by the background. This effect occurs most prominently in the opposite sign dilepton state, where the $t\bar{t}$ background dominates with almost 90% of the events, and both of our signal processes representing less than 1% of the total events, despite this final state being dominate for the processes individually.

The same sign dilepton region however shows promise for $t\bar{t}W$. The largest background process $t\bar{t}$ doesn't contribute in this final state, and WZ becomes the predominant background with approximately 75% of the events. Our combined signal in this region is approximately 22% with 21% coming from $t\bar{t}W$. While still smaller than the background our signal now contains almost a fourth of all events in this final state, which is a noticeable contribution, and thus this region would be a viable

Decay	$t\bar{t}$	$t\bar{t}W$	$t\bar{t}Z$	WZ	ZZ
$\sigma(pb)$	252.9000	0.2320	0.2060	20.3000	7.2000
ll	0.8905	0.0018	0.0011	0.0638	0.0428
$l^{\pm}l^{\mp}$ (OS)	0.8930	0.0012	0.0010	0.0618	0.0429
$e^{\pm}e^{\mp}$	0.8156	0.0011	0.0013	0.1067	0.0753
$e^{\pm}\mu^{\mp}$	0.9889	0.0014	0.0007	0.0063	0.0028
$\mu^{\pm}\mu^{\mp}$	0.8127	0.0011	0.0013	0.1084	0.0765
$l^{\pm}l^{\pm}$ (SS)	0.0000	0.2136	0.0115	0.7587	0.0163
$e^{\pm}e^{\pm}$	0.0000	0.2124	0.0115	0.7597	0.0163
$e^{\pm}\mu^{\pm}$	0.0000	0.2137	0.0115	0.7586	0.0163
$\mu^{\pm}\mu^{\pm}$	0.0000	0.2149	0.0115	0.7573	0.0163
lll	0.0000	0.0096	0.0147	0.9354	0.0402
$OSlll$	0.0000	0.0096	0.0147	0.9354	0.0402
$OSeee$	0.0000	0.0050	0.0145	0.9397	0.0408
$OSee\mu$	0.0000	0.0141	0.0149	0.9313	0.0398
$OSe\mu\mu$	0.0000	0.0138	0.0149	0.9310	0.0403
$OS\mu\mu\mu$	0.0000	0.0049	0.0145	0.9404	0.0401
$SSlll$	nan	nan	nan	nan	nan

Table 7: Relative event ratios between processes at $\sqrt{s} = 8$TeV with $N_{bjets} \geq 0$ and $p_T > 0$

option for analyses on $t\bar{t}W$. The best region for $t\bar{t}Z$ without taking the number of b-jets into account is the trilepton final state, however it still only contributes about 1.5% of the events.

The best final states become more apparent when the number of b-jets is taken into account. Table 8, shows the results for when $N_{bjets} = 2$ and Figure 2 shows a graphical breakdown of all comparisons by N_{bjets}. After applying this condition on N_{bjets}, the two remaining background processes of WZ and ZZ also drop out of the two regions identified as promising above. Now in the same sign dilepton region $t\bar{t}W$ dominates, contributing almost 95% of the events. $t\bar{t}Z$ is now dominate in the trilepton final state, contributing about 60% of all of the events. Figure 2 also shows that $t\bar{t}Z$ is the only process that produces more than two b-jets in a final state (opposite sign dilepton). It is also of interest to note that none of the processes produce a final state with exactly 1 b-jet. The best theoretical regions for studying our two signal processes are then the same sign dilepton final state with 2 b-jets for $t\bar{t}W$ and the trilepton state for $t\bar{t}Z$ with 2 b-jets as well as the opposite sign dilepton

Decay	$t\bar{t}$	$t\bar{t}W$	$t\bar{t}Z$	WZ	ZZ
$\sigma(pb)$	252.9000	0.2320	0.2060	20.3000	7.2000
ll	0.9875	0.0020	0.0011	0.0000	0.0095
$l^{\pm}l^{\mp}$ (OS)	0.9882	0.0014	0.0010	0.0000	0.0095
$e^{\pm}e^{\mp}$	0.9792	0.0013	0.0015	0.0000	0.0180
$e^{\pm}\mu^{\mp}$	0.9975	0.0014	0.0006	0.0000	0.0006
$\mu^{\pm}\mu^{\mp}$	0.9788	0.0013	0.0015	0.0000	0.0184
$l^{\pm}l^{\pm}$ (SS)	0.0000	0.9489	0.0511	0.0000	0.0000
$e^{\pm}e^{\pm}$	0.0000	0.9485	0.0515	0.0000	0.0000
$e^{\pm}\mu^{\pm}$	0.0000	0.9489	0.0511	0.0000	0.0000
$\mu^{\pm}\mu^{\pm}$	0.0000	0.9493	0.0507	0.0000	0.0000
lll	0.0000	0.3951	0.6049	0.0000	0.0000
$OSlll$	0.0000	0.3951	0.6049	0.0000	0.0000
$OSeee$	0.0000	0.2568	0.7432	0.0000	0.0000
$OSee\mu$	0.0000	0.4859	0.5141	0.0000	0.0000
$OSe\mu\mu$	0.0000	0.4815	0.5185	0.0000	0.0000
$OS\mu\mu\mu$	0.0000	0.2532	0.7468	0.0000	0.0000
$SSlll$	nan	nan	nan	nan	nan

Table 8: Relative event ratios between processes at $\sqrt{s} = 8$TeV with $N_{bjets} = 2$ and $p_T > 0$

state with more than 2 b-jets.

Finally it is also important to take into consideration the effects that the η and p_T cuts have on these distributions. Table 9 shows the comparison between the signal and background processes, after all cuts have been taken into account, for $N_{bjets} \geq 0$. Under these conditions, the same sign dilepton region begins to look less promising with the $t\bar{t}W$ percentage dropping down to only 7% from the previous 20% before cuts. This is due primarily to a large number of previously trilepton events from WZ migrating into the dilepton regions when they lose a single lepton to the cuts. Our signal processes are almost negligible in all other final state regions, with $t\bar{t}Z$ contributing only 1.5% in in the trilepton region and same sign dilepton region. All other signal regions are under 1%. However, adding in conditions on the number of b-jets in the final states once again is able to separate out our signal processes from the larger cross-section backgrounds. Table 10 shows the final state breakdowns across the processes for $N_{bjets} = 2$ and Figure 3 shows plots of the distributions of each final state for all categories of N_{bjets}. As before cuts were applied, imposing

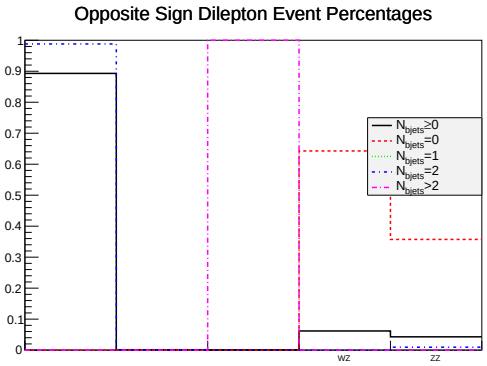

(a) Opposite Sign Dilepton

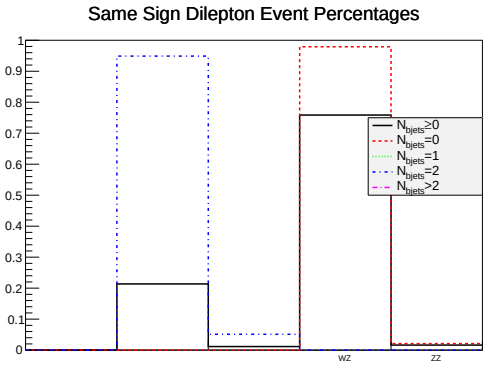

(b) Same Sign Dilepton

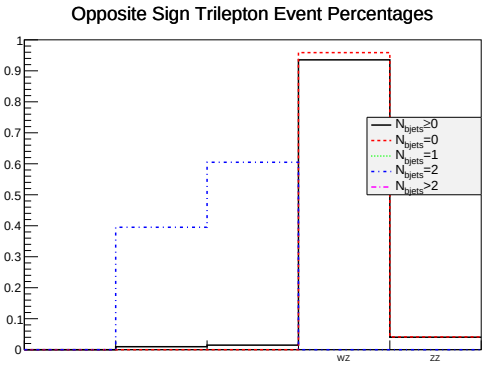

(c) Opposite Sign Trilepton

Figure 2: Theoretical Percentage comparisons for all event types and N_{bjets} categories

the condition that $N_{bjets} = 2$ removes the background processes in both the same sign dilepton and the trilepton final states with $t\bar{t}W$ dominating the same sign region with 83% of events and $t\bar{t}Z$ the main process in the trilepton final state with 67% of events. With cuts applied there are now also events that have exactly one b-jet, caused from a b-jet being lost due to the cuts. As expected the distributions for $N_{bjets} = 1$ closely follow the distributions for $N_{bjets} = 2$ as the only contributions to this final state will be from events that lost a b-jet in the cuts. However this now gives another region worth looking at to find our signal processes.

In summary, the best theoretical final states to look for our signal processes of $t\bar{t}W$ and $t\bar{t}Z$ are the same sign dilepton and trilepton final states under the condition that there are also two b-jets in the events. When cuts are applied the constraints

Decay	$t\bar{t}$	$t\bar{t}W$	$t\bar{t}Z$	WZ	ZZ
$\sigma(pb)$	252.9000	0.2320	0.2060	20.3000	7.2000
ll	0.8604	0.0019	0.0014	0.0874	0.0488
$l^{\pm}l^{\mp}$ (OS)	0.8681	0.0013	0.0013	0.0807	0.0487
$e^{\pm}e^{\mp}$	0.7793	0.0012	0.0017	0.1339	0.0839
$e^{\pm}\mu^{\mp}$	0.9806	0.0015	0.0008	0.0133	0.0038
$\mu^{\pm}\mu^{\mp}$	0.7783	0.0012	0.0017	0.1343	0.0845
$l^{\pm}l^{\pm}$ (SS)	0.0000	0.0731	0.0144	0.8462	0.0664
$e^{\pm}e^{\pm}$	0.0000	0.0696	0.0144	0.8459	0.0701
$e^{\pm}\mu^{\pm}$	0.0000	0.0730	0.0144	0.8463	0.0664
$\mu^{\pm}\mu^{\pm}$	0.0000	0.0767	0.0143	0.8461	0.0629
lll	0.0000	0.0076	0.0158	0.8440	0.1326
$OSlll$	0.0000	0.0076	0.0158	0.8440	0.1326
$OSeee$	0.0000	0.0039	0.0152	0.8414	0.1395
$OSee\mu$	0.0000	0.0111	0.0165	0.8457	0.1267
$OSe\mu\mu$	0.0000	0.0110	0.0164	0.8349	0.1377
$OS\mu\mu\mu$	0.0000	0.0039	0.0152	0.8539	0.1270
$SSlll$	nan	nan	nan	nan	nan

Table 9: Relative event ratios between processes at $\sqrt{s} = 8$TeV with $N_{bjets} \geq 0$ and $p_T > 25$

on b-jets can also be extended to include final states with either one or two b-jets.

6.2 Distinguishing $t\bar{t}W$ and $t\bar{t}Z$ from Background

Now that we have an idea of which final states to look at for our signal (same sign dilepton, and opposite sign trilepton), we turn to finding ways of distinguishing processes from one another within a given final state. In order to accomplish this we look at the kinematic properties of the particles created from the different processes using truth level information from Monte Carlo generated samples. For this section all samples will use the cuts presented in Section 5.2. We also require that $N_{bjets} > 0$ for all samples to remove the background processes of WZ and ZZ from the events.

The results of the previous section suggest that a strong variable to look at first would be N_{bjets} and also the similar variable of N_{jets}. Figure 4 and Figure 5 show the distributions for N_{bjets} and N_{jets} for all final states respectively.

The distributions for N_{bjets} are unfortunately similar for all three main processes

Decay	$t\bar{t}$	$t\bar{t}W$	$t\bar{t}Z$	WZ	ZZ
$\sigma(pb)$	252.9000	0.2320	0.2060	20.3000	7.2000
ll	0.9878	0.0022	0.0015	0.0000	0.0085
$l^{\pm}l^{\mp}$ (OS)	0.9887	0.0015	0.0014	0.0000	0.0085
$e^{\pm}e^{\mp}$	0.9803	0.0015	0.0020	0.0000	0.0162
$e^{\pm}\mu^{\mp}$	0.9973	0.0015	0.0007	0.0000	0.0005
$\mu^{\pm}\mu^{\mp}$	0.9801	0.0015	0.0020	0.0000	0.0164
$l^{\pm}l^{\pm}$ (SS)	0.0000	0.8357	0.1643	0.0000	0.0000
$e^{\pm}e^{\pm}$	0.0000	0.8281	0.1719	0.0000	0.0000
$e^{\pm}\mu^{\pm}$	0.0000	0.8355	0.1645	0.0000	0.0000
$\mu^{\pm}\mu^{\pm}$	0.0000	0.8430	0.1570	0.0000	0.0000
lll	0.0000	0.3244	0.6756	0.0000	0.0000
$OSlll$	0.0000	0.3244	0.6756	0.0000	0.0000
$OSeee$	0.0000	0.2054	0.7946	0.0000	0.0000
$OSee\mu$	0.0000	0.4017	0.5983	0.0000	0.0000
$OSe\mu\mu$	0.0000	0.4015	0.5985	0.0000	0.0000
$OS\mu\mu\mu$	0.0000	0.2064	0.7936	0.0000	0.0000
$SSlll$	nan	nan	nan	nan	nan

Table 10: Relative event ratios between processes at $\sqrt{s} = 8$TeV with $N_{bjets} = 2$ and $p_T > 25$

in the opposite sign dilepton final state, and our two signal processes also match in the remaining two states where $t\bar{t}$ drops out. N_{jets} however, does have distinguishing power. In the opposite sign dilepton state N_{jets} can be broken into three distinct regions: $N_{jets} < 3$ where all three processes are abundant, $3 \leq N_{jets} \leq 5$ where there is only our two signal processes, and $N_{jets} > 5$ where there is only $t\bar{t}Z$. The trilepton final state can be similarly broken down into two regions, $N_{jets} \leq 2$, where $t\bar{t}W$ dominates $t\bar{t}Z$ and $N_{jets} > 2$ where only $t\bar{t}Z$ is present. The distributions in the same sign dilepton region are approximately the same, and would not be good for distinguishing events.

The next kinematic variable we looked at is MET. For this calculation the MET was estimated as the vector sum of the p_T of all of the high energy objects in the event (jets and leptons) that passed the imposed cuts. The distributions for the MET is given in Figure 6. The MET is able to distinguish well between $t\bar{t}Z$ and the other processes in the opposite sign dilepton final state, and slightly in the trilepton state, however in the same sign dilepton state, the distributions of our two signal

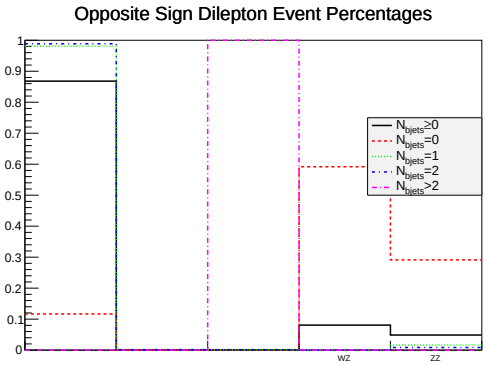

(a) Opposite Sign Dilepton

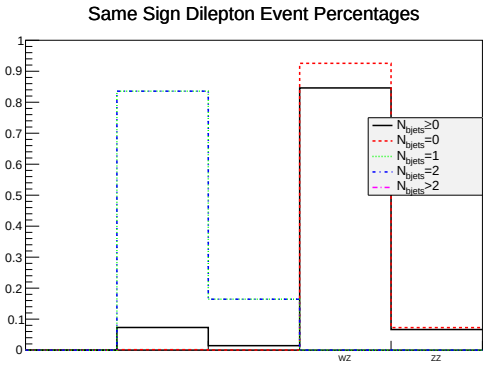

(b) Same Sign Dilepton

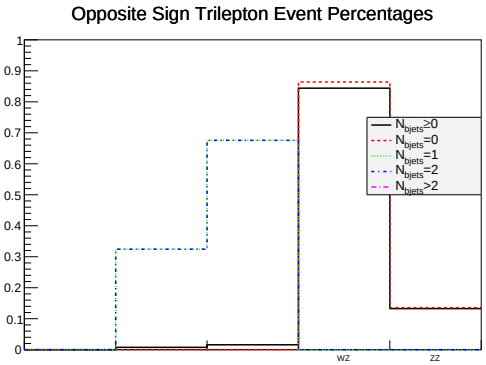

(c) Opposite Sign Trilepton

Figure 3: Theoretical Percentage comparisons for all event types and N_{bjets} categories after all cuts have been applied

processes are roughly the same.

Another variable of interest is the distance between the two leading leptons in the events (ΔR) shown in Figure 7. Again $t\bar{t}Z$ has a distinguishable shape from the other processes in the opposite sign dilepton and trilepton final states, but not in the same sign dilepton state. This appears to be reasonable as about half of opposite sign dilepton events would have both leptons coming from the Z boson, and thus would be expected to be closer together than if they were the decay products of two separate particles, which is what we observe. This is even more pronounced in the trilepton final state, where an even larger percentage of leptons will come from the Z decay, and completely absent from the same sign dilepton channel where one lepton

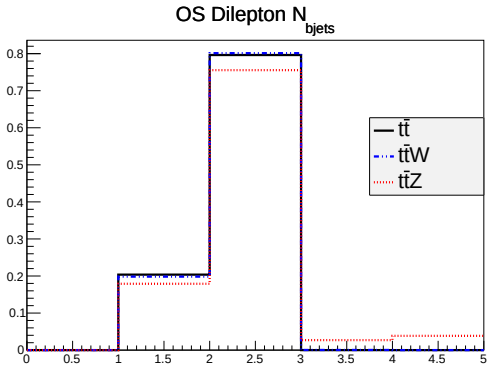

(a) Opposite Sign Dilepton

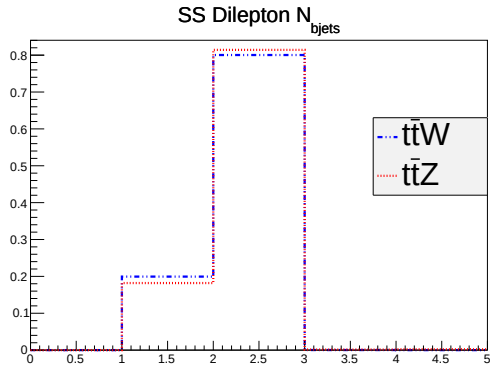

(b) Same Sign Dilepton

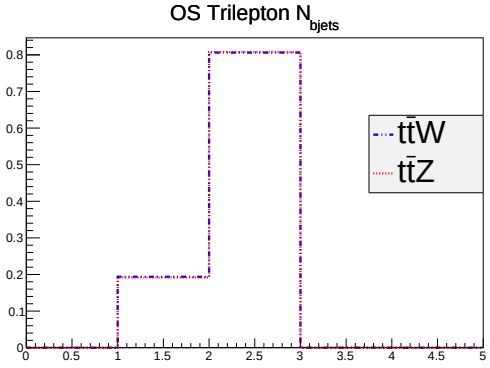

(c) Opposite Sign Trilepton

Figure 4: Distribution of N_{bjets}

must come from one of the top quarks and one for the Z.

Once we have identified a number of kinematic quantities we can also start to combine them to create different phase spaces that can distinguish between our processes, as well as feed them into a neural network for a more optimal separation.

7 Conclusion

From our analysis of the branching ratios for each of our signal and background processes we were able to determine that the best final states to look at were the same sign dilepton and the trilepton regions. The primary background process of $t\bar{t}$ only contributes to the opposite sign dilepton region, making measurements in

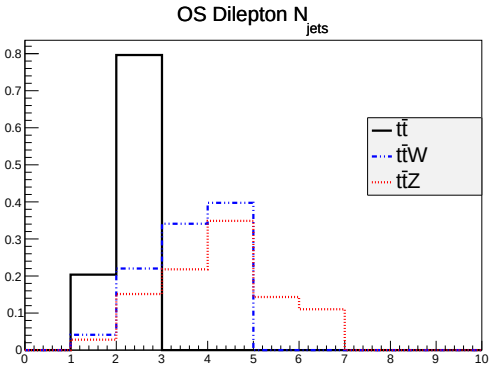

(a) Opposite Sign Dilepton

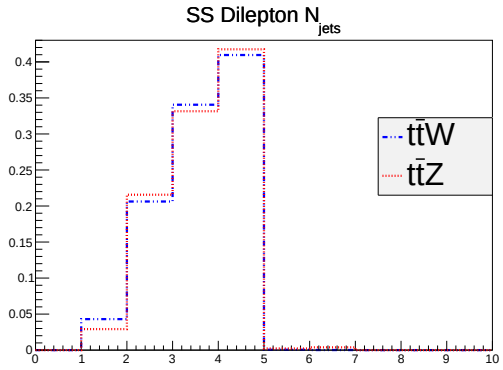

(b) Same Sign Dilepton

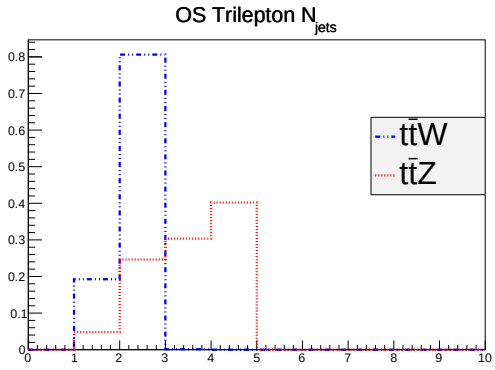

(c) Opposite Sign Trilepton

Figure 5: Distribution of N_{jets}

the final state to be difficult. Furthermore adding in a requirement that $N_{bjets} > 0$ will remove the remaining background processes of WZ and ZZ from the regions of interest. Turning to Monte Carlo simulations we found kinematic quantities that could be used to distinguish our processes from each other. We found that our two processes had similar kinematic distributions in the same sign dilepton final state. We conclude that this would work well if the primary concern of an analysis is looking for $t\bar{t}V$ where V is either a W or Z boson, but does not care to distinguish between the two, as the same sign dilepton region has a larger branching ratio the the trilepton region. The trilepton region however has a number of kinematic quantities that differ between our two signal processes (N_{jets}, MET, ΔR between leading leptons), and these quantities can be used to distinguish well between $t\bar{t}W$ and $t\bar{t}Z$.

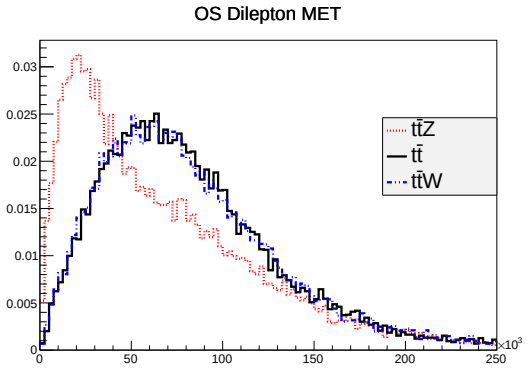

(a) Opposite Sign Dilepton

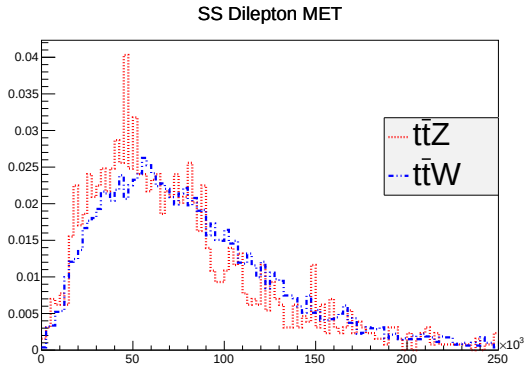

(b) Same Sign Dilepton

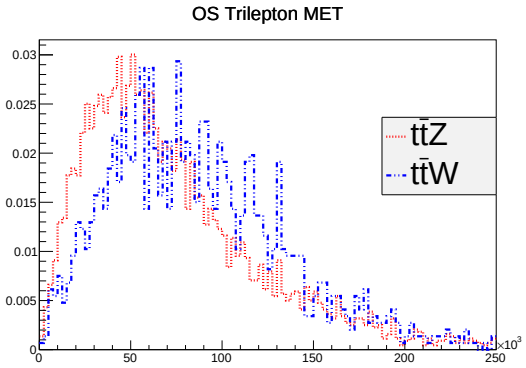

(c) Opposite Sign Trilepton

Figure 6: Distribution of MET for all processes

It is important to remember that the results found in this study are much cleaner than would be expected from an analysis on data collected from the ATLAS detector. This is due to the fact that this study looks only at the differences between the processes directly, from branching ratios and Monte Carlo truth data, but does not take into account many of the outside factors that can obscure the data. These factors primarily come from two main sources: errors introduced due to the physical nature of the detector, and secondary events. Both of these sources of error are difficult to calculate from a theoretical framework, and often rely on data driven estimates. The major errors caused by the detector itself come from particles or kinematic quantities being misidentified or miss measured. These include jets being misidentified as electrons (fakes) and electron charges being flipped by kinks in the

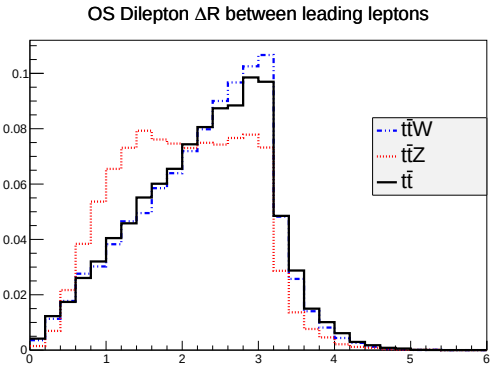

(a) Opposite Sign Dilepton

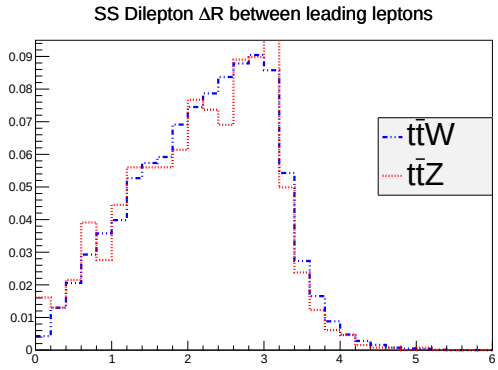

(b) Same Sign Dilepton

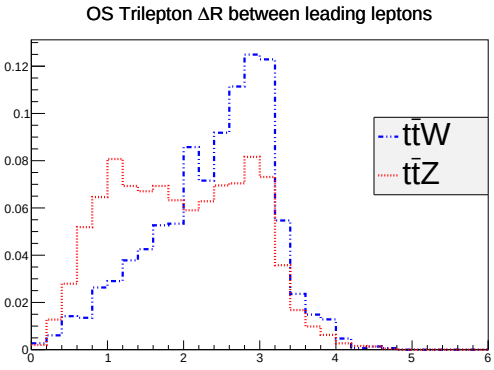

(c) Opposite Sign Trilepton

Figure 7: Distribution of ΔR between leading leptons for all processes

electron track due to Bremsstrahlung radiation (charge flips), which change the final states of the events recorded. Other errors can be introduced from secondary events and QCD radiation that introduce additional jets and other particles clouding our signal regions. The clouding effects of theses phenomena would most likely require a more sophisticated method of distinguishing between events. To this end, kinematic quantities, such as those presented here, could be given as inputs for a neural network or boosted decision tree, which take into account correlations between variables, to give better separation of signal and background. A full data analysis would need to be able to take these additional factors into account, however this study acts as a useful starting platform for a large and more in-depth study.

References

[1] D. Griffiths, *Introduction to Elementary Particles*. John Wiley & Sons, INC., New York, 2nd Edition, 2008

[2] ATLAS Collaboration *Evidence for the associated production of a vector boson (W,Z) and top quark pair in the dilepton and trilepton channels in pp collision data at sqrts = 8 TeV by the ATLAS detect at the LHC* ATLAS-CONF-2014-038

[3] CMS Collaboration *Measurement of top quark-antiquark pair production in association with a W or Z boson in pp collisions at sqrts = 7 TeV* CMS-TOP-12-036

[4] ATLAS Collaboration *Simultaneous measurements of the $t\bar{t}, W^+W^-, and Z/\gamma^* \rightarrow \tau\tau$ production cross-sections in pp collisions at sqrts = 7 TeV with the ATLAS detector* CERN-PH-EP-2014-119

[5] K. A. Olive *et al.* [Particle Data Group Collaboration], "Review of Particle Physics,' Chin. Phys. C **38**, 090001 (2014).